

## Electron-impact excitation of electronic states in argon at incident energies between 16 and 100 eV

A. Chutjian

*Jet Propulsion Laboratory, California Institute of Technology, Pasadena, California 91109*

D. C. Cartwright

*Theoretical Division, Los Alamos Scientific Laboratory, Los Alamos, New Mexico 87545*

(Received 13 May 1980)

Normalized, absolute differential cross sections have been measured for electron-impact excitation of 23 individual or composite electronic states of argon lying within 14.30 eV of the ground state. Incident electron energies are 16, 20, 30, 50, and 100 eV, and the range of scattering angles  $5^\circ$ – $138^\circ$ . The absolute differential cross sections are extrapolated to  $0^\circ$  and  $180^\circ$  and integrated to yield integral and inelastic-scattering momentum-transfer cross sections for the excitation processes. Errors in the differential cross section are grouped into the classes *A* (26%), *B* (31%), and *C* (45%), with slightly larger errors given to the integrated quantities owing to extrapolation uncertainties. Comparisons of the present data are made with previous measurements where available, and with results of several distorted-wave and Born calculations. Differential magnetic sublevel cross sections for the  $^3P_1$  and  $^1P_1$  levels are also obtained at 50-eV incident energy and  $5^\circ$  scattering angle using previously measured  $\lambda$  parameters.

### I. INTRODUCTION

Because of its presence in high concentration, argon atoms play a major role in the performance of the high-pressure Ar-Kr-F<sub>2</sub> laser system<sup>1</sup> and in direct nuclear-pumped lasing media using He-Ar mixtures.<sup>2,3</sup> Absolute electron-impact integral and differential cross sections, both elastic and inelastic, are needed to carry out theoretical studies of modeling and output optimization.<sup>4</sup> Inelastic cross sections provide, for example, rates of electron energy degradation via argon line radiation and metastable state formation. Such degradation rates are also found to be important in calculating electron-energy distribution functions for Ar-N<sub>2</sub>-SF<sub>6</sub> mixtures used as gaseous insulators.<sup>5</sup>

In the present study the technique of low-energy electron scattering is used to obtain normalized, absolute, differential inelastic cross sections in argon.<sup>6</sup> Integral and momentum-transfer cross sections are obtained from these differential results. The electronic states studied lie within 14.30 eV of the ground state. There are 30 states in this energy region<sup>7</sup> of which 18 are resolved in the present measurements. The angular range ( $\theta$ ) covered is  $5^\circ$  to  $138^\circ$ , and the electron energies ( $E_0$ ) are 16, 20, 30, 50, and 100 eV. This range in energy spans the peaks of the cross sections, and the highest energy (100 eV) is approximately seven times the threshold of the highest energy-loss feature. Thus, semiempirical or Born-type approximations can be used to extend data to higher electron energies if necessary.

The present cross sections are also useful to

theoreticians who may wish to test particular  $e$ -atom scattering approximations in this (theoretically difficult) low-to-intermediate electron energy regime because they are both cascade free and differential in nature. It often happens, for example, that a theory which successfully accounts for only the low-angle portion of a steeply descending differential cross section (DCS) gives a satisfactory integral cross section (ICS), but an incorrect inelastic momentum-transfer cross section. A comparison against the entire DCS shows whether theory adequately describes the excitation process throughout the entire angular range.

Previous *relative* DCS measurements<sup>8</sup> in argon have been made of the  $3p \rightarrow 4s$  excitations (levels 1–4, see Table I), and  $3p \rightarrow 4p$  excitations (levels 5, 7, and 14). The incident electron energy was 30 and 50 eV and the angular range  $0^\circ$ – $90^\circ$ . Relative cross sections have also been measured<sup>9</sup> for the unresolved levels 1–4 at  $\theta$  between  $0^\circ$  and  $140^\circ$  at  $E_0$  between 30 and 120 eV; and for two levels ( $3d[1/2]_1^0$  and  $3d[7/2]_4^0$ , the first of which was unresolved in the present work) only partially resolved at energies of 30 and 98 eV.<sup>10</sup> Finally, several energy-loss spectra have been reported under (“optical-like”) conditions of high electron energy and low scattering angle,<sup>11</sup> but no absolute or relative cross sections were given at these energies.

Considerable work has been done on the electron-impact excitation of the first four levels in argon, two of which are metastable [levels 1 and 3 for which  $\Delta J=2$  and 0 (since  $0 \neq 0$ )]; and two of which radiate to the ground state (levels 2 and 4,  $\Delta J=1$ ). The excitation function of metastables

has been measured from threshold to 10 eV (relative)<sup>12</sup> and to 150 eV (relative),<sup>13</sup> threshold to 200 eV (relative)<sup>14</sup> and threshold to 50 eV (absolute).<sup>15</sup> Apparent excitation functions have been measured for higher-lying states as well, with corrections for cascading made in some cases.<sup>16</sup> For the resonance lines measurements have been made<sup>17,18</sup> of absolute cross sections for the resolved levels 2 and 4, as well as of the scattering parameters<sup>19,20</sup>  $\lambda$  and  $\chi$ . From the definition of  $\lambda$  and the present DCS measurements one is also able to obtain absolute magnetic sublevel cross sections for each line, as was done for levels in helium.<sup>21</sup>

Theoretical results which are pertinent to the present measurements include a combination of the Born approximation and experimental generalized oscillator strengths to get a set of semiempirical cross sections for plasma modeling purposes.<sup>22</sup> *Ab initio* results include those obtained using the distorted wave theory,<sup>23</sup> the Born approximation using both single and multiconfiguration Hartree-Fock wave functions,<sup>24</sup> and the many-body formulation.<sup>25,26</sup> Comparisons to results of these theories will be made in Section III.

## II. EXPERIMENTAL CONSIDERATIONS

The experimental techniques used in the present measurements, including the method of deconvoluting spectral lines, have been described earlier<sup>27</sup> in comparable inelastic measurements of  $N_2$  so that only a brief survey will be given here.

A beam of monoenergetic electrons is focused onto the target argon atoms effusing from a multichannel capillary array. Inelastic electrons at some  $\theta$  are energy analyzed, detected, and the signal versus energy loss stored in a multichannel scaler. The energy analyzer was designed to focus electrons at the input plane of the hemispherical deflector with zero beam angle, of fixed energy, independent of the scattered electron energy.<sup>28</sup> This feature made it possible to measure reliable relative intensities among the different inelastic features, and also reliable inelastic-to-elastic intensity ratios.

By a combination of good electron energy resolution (38–55 meV full width at half maximum) and the use of a tested deconvolution procedure, it was possible to obtain DCS's for 23 electronic features, of which only five consisted of a blend of two or more lines (see Table I). In several cases (lines 6, 7 and 8, 9) individual features were separated by the deconvolution technique which are only 19 meV apart.

The normalization procedure to the absolute cross-section scale proceeded in much the same way as in work on  $N_2$ .<sup>27</sup> First, the inelastic ener-

TABLE I. Correspondence of level numbers used in the present work with argon spectral line designations (Ref. 7).

Level number	Line
1	$4s[3/2]_2^0 \ ^3P_2$
2	$4s[3/2]_1^0 \ ^3P_1$
3	$4s'[1/2]_0^0 \ ^3P_0$
4	$4s'[1/2]_1^0 \ ^1P_1$
5	$4p[1/2]_1$
6	$4p[5/2]_3$
7	$4p[5/2]_2$
8	$4p[3/2]_1$
9	$4p[3/2]_2$
10	$4p[1/2]_0$
	$4p'[3/2]_1$
11	$4p'[3/2]_2$
12	$4p'[1/2]_1$
13	$4p'[1/2]_0$
14	$3d[1/2]_0^0$
	$3d[1/2]_1^0$
15	$3d[3/2]_2^0$
16	$3d[7/2]_4^0$
17	$3d[7/2]_3^0$
18	$3d[5/2]_2^0$
	$5s[3/2]_2^0$
19	$3d[5/2]_3^0$
	$5s[3/2]_1^0$
20	$3d[3/2]_1^0$
21	$3d'[5/2]_2^0$
22	$3d'[3/2]_2^0$
	$3d'[5/2]_3^0$
	$5s'[1/2]_0^0$
	$5s'[1/2]_1^0$
23	$3d'[3/2]_1^0$

gy-loss spectrum at a particular  $E_0$  and  $\theta$  was deconvoluted, and peak intensities (as measured by areas) obtained relative to the (usually) strongest feature—feature 4. In a separate set of runs the ratio of feature 4 area to the area of the elastic-scattering feature was measured. At low scattering angles care was given to the contribution of the parent beam itself to the elastic feature. In all cases measurements were made to

that smallest  $\theta$  where this correction did not exceed about 15%. Finally, using the absolute elastic DCS reported in the previous paper,<sup>29</sup> the inelastic feature 4 was placed on the absolute scale, by which all the other inelastic features could be made absolute.

It is difficult to discuss errors related to each data point since over  $10^3$  points were obtained in these measurements. Rather a "level of error" which applies to each numbered feature is given. This level of error takes into account the following individual errors:

- (a) error in the deconvolution of each feature from nearby features;
- (b) error in converting, at each energy and angle, to an intensity relative to the elastic-scattering intensity;
- (c) error in the elastic differential scattering cross section.

For integral cross sections an additional error is involved, namely,

- (d) error in extrapolation of the measured DCS to  $0^\circ$  and  $180^\circ$ .

These four "steps" in the data analysis were considered independent so that the overall error in the DCS is taken as the quadrature (root-mean-square) sum of errors in (a), (b), and (c). Included in that sum for the integral and momentum-transfer cross section is the extrapolation error of (d). Errors in (b) and (c) are taken as 15% and 20%, respectively, giving an "intrinsic" error in the DCS of 25%. The main variation in the level of error of each DCS is determined by (a), i.e., the strength and degree of resolution of the feature in the original data. This deconvolution error can be grouped into three classes: (A) 10% or less, (B) 10–25%, (C) 26–50%. This gives rise to an average root-mean-square error for (a), (b), and (c) of 26%, 31%, and 45%, respectively. The error due to extrapolation (d) for the integral ( $\sigma_I$ ) and momentum-transfer ( $\sigma_M$ ) cross sections is estimated to be 12% and 16%, respectively. They were arrived at by taking various extrapolations to  $0^\circ$  and  $180^\circ$ , using theoretical DCS's as a guide where available, and calculating the variations in  $\sigma_I$  and  $\sigma_M$ . As a summary, the classes of errors are

Class	Deconvolution error (%)	DCS error (%)	$\sigma_I$ error (%)	$\sigma_M$ error (%)
A	<10	26	29	31
B	10–25	31	33	35
C	26–50	45	47	48

The appropriate class is given at the bottom of each column in Tables II–X.

### III. RESULTS AND DISCUSSION

Typical energy-loss spectra are shown in Fig. 1 at the indicated scattering angles and electron energies. Rydberg series in the  $s$ ,  $p$ ,  $d$  and  $s'$ ,  $p'$ ,  $d'$  orbitals corresponding to  $^2P_{3/2}$  and  $^2P_{1/2}$  states of the Ar II core are also indicated. The spectra marked DATA are raw spectra, while the CALC spectra are computer-generated "best-fit" spectra. The spectrum DIF (DC) corresponds to the difference between the calculated and measured spectra. Further spectral fitting details may be found in Ref. 27. In Fig. 2 we show a simplified Grotrian-type energy level diagram<sup>30</sup> of the argon energy levels where again primed and unprimed series of levels correspond to the  $^2P_{1/2}$  and  $^2P_{3/2}$  cores of Ar II, respectively.

#### A. Differential cross sections

Results such as those shown in Fig. 1 give intensities of each spectral feature relative to that of feature 4. In order to convert these inelastic-to-inelastic ratios to inelastic-to-elastic ones, a measurement of the intensity of feature 4 to that for elastic scattering was carried out at each  $E_0$  and  $\theta$  for which inelastic data were obtained. The results of these measurements are shown in Figs. 3 and 4 at the indicated energies and scattering angles. Data were taken in both a multichannel scaling mode (in which the entire elastic and level 4 peaks were recorded) and single-channel mode (only peak intensities recorded). Low-angle data ( $\theta < 20^\circ$ ) were corrected for any parent beam effects. Measurements were continued to successively lower scattering angles until this correction exceeded 15%.

Since all inelastic intensities were determined relative to the elastic scattering intensity, multiplication of this ratio by the elastic argon DCS<sup>29</sup> gives the absolute inelastic DCS for each feature. Experimental and recent first-order many-body theory (FOMBT) results for 16-eV incident energy are shown for the metastable levels 1 and 3 in Fig. 5, and for the optically allowed levels 2 and 4 in Fig. 6. The level numbering scheme in Table I has been used as a shorthand notation for the excited-state levels in all the figures in order to avoid repetition of the longer spectroscopic notation.

In the FOMBT approximation for electron impact excitation the scattering  $T$  matrix includes both direct and exchange scattering, and distorted waves for both incident and scattered electrons are calculated in the field of the *ground state* of

TABLE II. Differential, integral ( $\sigma_I$ ), and momentum-transfer ( $\sigma_M$ ) cross sections for levels 1 and 2. In this and following tables the first line of the column heading is the incident energy (eV), the second line the level number, and the third the cross-section multiplier ( $\text{cm}^2/\text{sr}$ ) for that column. Entries at angles given in parentheses refer to extrapolated cross sections.

Angle (deg)	16		20		30		50		100	
	1 ( $10^{-18}$ )	2 ( $10^{-18}$ )	1 ( $10^{-18}$ )	2 ( $10^{-18}$ )	1 ( $10^{-18}$ )	2 ( $10^{-18}$ )	1 ( $10^{-20}$ )	2 ( $10^{-18}$ )	1 ( $10^{-21}$ )	2 ( $10^{-18}$ )
(0)	1.70	20.2	6.40	25.2	4.15	159	10.2	522	152	690
10	0.951	13.2	3.94	14.8	5.60	72.0	14.5	152	77.0	75.7
20	0.860	4.41	2.40	6.00	5.80	20.8	13.8	18.7	31.5	3.50
30	1.03	2.30	2.45	3.12	4.75	7.75	10.7	6.25	10.2	1.85
40	1.41	1.87	2.58	2.69	3.45	5.00	7.20	3.85	2.75	0.790
50	2.30	2.29	2.14	2.51	1.59	3.15	3.68	1.95	1.43	0.280
60	2.85	2.70	1.95	2.90	0.360	1.50	1.53	0.745	1.19	0.115
70	3.20	2.52	1.79	2.20	0.101	0.600	1.19	0.470	1.40	0.103
80	3.20	2.09	1.61	1.49	0.189	0.780	1.31	0.610	1.89	0.168
90	3.08	2.14	1.51	1.37	0.355	1.04	1.50	0.760	2.17	0.215
100	2.95	2.50	1.70	1.65	0.400	1.09	1.69	0.860	2.02	0.141
110	2.91	2.98	2.03	2.19	0.405	0.925	1.80	0.830	1.61	0.071
120	3.12	3.38	2.50	2.72	0.415	0.720	1.60	0.640	1.10	0.033
130	3.80	3.97	3.10	3.30	0.605	0.800	1.02	0.315	0.910	0.029
140	5.60	4.44	3.90	3.92	1.31	1.31	0.785	0.124	1.35	0.061
(150)	7.30	4.78	4.90	4.57	2.15	2.05	1.09	0.255	2.09	0.128
(160)	8.80	5.00	6.00	5.24	3.12	2.95	1.73	0.541	3.05	0.229
(170)	10.2	5.18	7.35	6.00	4.12	4.25	2.63	0.960	4.35	0.345
(180)	11.3	5.30	8.90	6.85	4.90	5.25	3.39	1.49	5.40	0.430
$\sigma_I$	41.9	39.7	31.9	37.0	16.6	45.6	36.1	57.8	56.0	32.8
$\sigma_M$	52.0	42.2	36.5	36.7	12.6	18.4	20.5	9.40	23.7	2.03
Error class	A	A	A	A	A	A	B	A	C	A
$\sigma_I^a$	45.4	36.6	78.7	78.4	46.4	81.9	54.0	71.5		
$\sigma_M^a$	45.8	34.9	72.6	64.7	33.9	45.7	48.8	18.8		
$\sigma_I(2+4)^b$		149		221		284		282		221

<sup>a</sup>Reference 25.

<sup>b</sup>Reference 24. The listed cross section is for the sum of levels 2 and 4 using the multiconfiguration Hartree-Fock wave function for the ground state and fully relaxed wave function for the excited state.

the Ar target. Spin-orbit coupling effects were included in the calculation of the scattering orbitals and transition density matrices.<sup>25</sup> Fairly good agreement, in both magnitude and shape, is found between theory and experiment, especially for excitation of the dipole-allowed levels 2 and 4 (see Figs. 7 and 8). The experimental undulations in the DCS's for all four levels are confirmed by theory, although the *phase* of the theoretical oscillation appears to differ from experiment somewhat more for excitation of the dipole forbidden levels (levels 1 and 3).

Comparison of the FOMBT and experiment at 20 eV is shown in Figs. 7 and 8, and at 30 eV in Figs. 9 and 10. Agreement in magnitude between theory and experiment seems to have worsened relative to that at 16 eV although agreement in shape is still fairly good. It should be noted that both theory and present data find a relative minimum in the DCS in the 70°–80° angular region which was not found in some earlier relative DCS

measurements<sup>6</sup> (shown by the filled and open triangles in Fig. 10, normalized to present absolute results at 40°).

The agreement between experiment and theory at 30 eV for excitation of the metastable levels 1 and 3 (Fig. 9) is about the same as at 20 eV. The principal difference between the present data and those of Ref. 8 (normalized again at 40°) shown in Fig. 9 appears to be in the depth of the minimum in the 70°–80° angular range. Results of the present measurements and the FOMBT at 50 eV incident energy are shown in Figs. 11 and 12 for levels 1, 3 and 2, 4, respectively. The data in these figures again illustrate the good agreement between experiments, and calculations in the FOMBT for the shape and magnitude of DCS for these four levels.

Tabulations of the DCS's (every 10°) are given in Tables II–X for the 23 features studied. It is understood that in some cases (see Fig. 12) certain deep, narrow minima may be missed by this

TABLE III. Same as Table II, but for levels 3 and 4.

Angle (deg)	16		20		30		50		100	
	3 (10 <sup>-20</sup> )	4 (10 <sup>-19</sup> )	3 (10 <sup>-20</sup> )	4 (10 <sup>-19</sup> )	3 (10 <sup>-20</sup> )	4 (10 <sup>-19</sup> )	3 (10 <sup>-21</sup> )	4 (10 <sup>-19</sup> )	3 (10 <sup>-21</sup> )	4 (10 <sup>-19</sup> )
(0)	5.05	75.0	23.0	77.0	11.2	490	91.5	1710	265	2650
10	2.75	43.0	11.4	46.0	13.2	250	72.5	585	89.0	290
20	2.15	14.1	4.46	16.9	13.0	67.0	52.0	76.3	23.8	13.4
30	2.13	6.39	5.10	6.74	10.4	22.0	34.5	22.7	15.0	6.90
40	2.59	3.62	4.70	5.93	6.70	13.3	19.7	14.5	3.65	3.05
50	3.60	4.43	3.70	6.75	3.02	8.45	10.0	7.30	1.39	1.00
60	4.95	4.70	4.20	7.95	0.940	4.48	6.20	2.43	0.951	0.460
70	5.80	4.30	4.15	5.60	0.440	2.15	4.40	1.61	1.00	0.477
80	5.80	2.95	3.47	2.60	0.380	2.49	3.20	2.11	1.24	0.847
90	5.30	2.77	3.07	2.13	0.385	2.98	2.90	2.59	1.41	0.842
100	5.10	3.48	3.48	3.15	0.460	3.35	2.95	2.80	1.40	0.664
110	5.22	5.30	4.05	4.65	0.685	2.63	3.30	2.59	1.30	0.389
120	5.78	6.70	4.98	5.70	0.845	1.72	3.40	1.81	1.12	0.152
130	6.80	7.95	6.18	6.98	1.49	1.95	2.90	0.910	0.975	0.100
140	8.50	10.3	7.90	10.7	5.65	3.21	2.92	0.440	0.980	0.209
(150)	10.4	12.9	9.60	15.0	10.2	6.81	3.75	0.745	1.20	0.435
(160)	12.4	15.0	11.3	20.2	14.9	11.8	5.15	1.44	1.67	0.790
(170)	13.9	16.9	13.2	24.9	19.2	16.9	6.70	2.59	2.29	1.19
(180)	15.3	18.8	15.2	28.5	24.0	19.8	8.40	3.99	2.89	1.49
$\sigma_I$	60.9	85.3	64.4	100	45.4	144	112	214	54.1	134
$\sigma_M$	65.8	90.0	72.7	98.2	46.1	57.4	53.2	31.1	17.8	8.21
Error class	B	A	B	A	C	A	C	A	C	A
$\sigma_I^a$	90.8	64.2	157	170	92.9	241	108	272		
$\sigma_M^a$	91.6	56.9	145	127	67.9	121	97.5	66.1		

<sup>a</sup>Reference 25.

TABLE IV. Same as Table II, but for levels 5 and 6.

Angle (deg)	20		30		50		100	
	5 (10 <sup>-19</sup> )	6 (10 <sup>-19</sup> )	5 (10 <sup>-19</sup> )	6 (10 <sup>-19</sup> )	5 (10 <sup>-20</sup> )	6 (10 <sup>-20</sup> )	5 (10 <sup>-21</sup> )	6 (10 <sup>-21</sup> )
(0)	5.20	1.01	39.0	69.0	8.40	110	120	480
10	2.95	0.780	29.5	43.5	4.82	44.5	57.0	270
20	1.39	0.460	17.5	24.8	2.58	10.0	5.00	37.0
30	0.256	0.310	7.60	13.4	1.28	3.65	1.98	3.30
40	0.120	1.14	2.10	8.80	0.650	2.00	1.52	1.12
50	0.730	1.72	3.09	4.75	0.520	1.37	1.49	0.600
60	1.51	2.20	4.95	7.30	1.24	1.02	1.72	0.540
70	0.890	0.560	5.21	6.18	6.00	0.981	2.00	0.641
80	0.285	0.465	4.15	3.35	3.30	1.21	2.41	0.792
90	0.133	0.655	2.30	2.62	0.400	1.63	2.89	0.961
100	0.790	1.03	1.62	3.02	0.330	1.93	3.39	1.17
110	1.53	1.43	4.15	4.05	0.920	1.92	3.85	1.39
120	1.69	1.90	5.60	6.05	1.52	1.52	4.35	1.61
130	1.70	2.85	2.72	11.1	1.39	0.960	4.80	1.89
140	1.72	4.30	1.68	20.2	0.870	0.510	5.25	2.15
(150)	1.75	5.90	2.30	28.8	0.738	0.625	5.70	2.35
(160)	1.80	7.70	3.50	38.0	1.24	1.13	6.15	2.58
(170)	1.90	9.30	4.90	48.0	1.88	1.98	6.55	2.79
(180)	2.10	10.1	6.20	58.0	2.31	2.89	6.95	2.99
$\sigma_I$	13.5	24.4	56.5	133	20.0	30.8	53.8	93.1
$\sigma_M$	15.9	33.9	43.0	153	17.2	16.9	50.6	21.2
Error class	A	B	B	B	C	C	C	C

TABLE V. Same as Table II, but for levels 7, 8, and 9.

Angle (deg)	20			30			50			100		
	7 (10 <sup>-19</sup> )	8 (10 <sup>-19</sup> )	9 (10 <sup>-19</sup> )	7 (10 <sup>-19</sup> )	8 (10 <sup>-20</sup> )	9 (10 <sup>-20</sup> )	7 (10 <sup>-20</sup> )	8 (10 <sup>-20</sup> )	9 (10 <sup>-20</sup> )	7 (10 <sup>-20</sup> )	8 (10 <sup>-20</sup> )	9 (10 <sup>-20</sup> )
(0)	3.45	1.60	2.91	14.0	74.0	131	495	149	415	490	64.0	475
10	3.00	1.10	2.55	11.1	59.5	89.5	281	87.0	235	220	33.0	195
20	2.30	0.619	2.05	7.70	38.5	54.0	111	17.0	94.0	19.2	4.10	16.2
30	1.42	0.300	1.38	4.50	13.1	32.6	23.0	5.70	18.7	4.40	1.29	4.35
40	0.894	0.435	0.838	2.09	5.90	17.4	9.35	2.82	8.15	2.85	0.710	3.60
50	1.00	0.665	0.878	1.19	5.05	8.95	5.00	1.81	4.55	1.60	0.540	1.37
60	1.16	0.490	0.920	0.750	4.61	4.50	2.35	1.32	1.90	0.781	0.500	0.250
70	0.970	0.120	0.850	0.440	3.42	3.45	1.92	1.13	1.64	0.579	0.535	0.290
80	0.750	0.120	0.730	0.358	2.05	3.69	2.89	0.955	3.09	0.561	0.600	0.395
90	0.638	0.350	0.632	0.540	1.79	4.75	3.81	0.775	3.41	0.610	0.680	0.460
100	0.770	0.595	0.630	0.540	1.93	3.98	4.12	0.615	3.09	0.591	0.771	0.375
110	0.970	0.760	0.720	0.260	2.41	2.32	3.60	0.570	2.49	0.482	0.861	0.255
120	1.00	1.05	0.820	0.345	3.35	2.22	2.80	0.639	1.91	0.291	0.963	0.160
130	0.970	1.80	1.29	0.890	5.58	3.78	1.80	0.800	1.37	0.182	1.08	0.120
140	0.980	2.90	1.86	1.42	9.85	6.78	0.900	1.14	1.39	0.225	1.19	0.112
(150)	1.03	4.05	2.48	1.97	15.1	11.6	0.880	1.62	2.51	0.355	1.29	0.131
(160)	1.19	5.05	3.20	2.55	21.0	17.9	1.61	2.33	5.00	0.520	1.39	0.170
(170)	1.32	6.10	4.00	3.25	25.9	24.0	3.05	3.15	8.30	0.685	1.45	0.229
(180)	1.49	7.00	4.95	3.90	28.2	28.2	4.60	3.98	11.0	0.870	1.50	0.300
$\sigma_I$	12.9	13.8	14.6	17.9	95.6	128	150	41.0	130	67.3	19.3	58.9
$\sigma_M$	11.9	20.7	16.5	12.6	84.6	82.0	38.5	14.8	38.8	7.62	11.9	5.08
Error class	A	B	B	B	B	B	B	C	B	B	C	B

TABLE VI. Same as Table II, but for levels 10, 11, and 12.

Angle (deg)	20			30			50			100		
	10 (10 <sup>-19</sup> )	11 (10 <sup>-19</sup> )	12 (10 <sup>-20</sup> )	10 (10 <sup>-19</sup> )	11 (10 <sup>-19</sup> )	12 (10 <sup>-20</sup> )	10 (10 <sup>-19</sup> )	11 (10 <sup>-20</sup> )	12 (10 <sup>-20</sup> )	10 (10 <sup>-20</sup> )	11 (10 <sup>-20</sup> )	12 (10 <sup>-20</sup> )
(0)	1.03	2.15	9.05	7.00	14.7	46.2	31.0	313	41.5	120	451	45.2
10	1.12	1.88	8.20	6.20	12.1	35.8	10.3	208	21.8	63.0	169	17.2
20	1.49	1.33	6.30	4.82	7.45	23.8	1.52	88.1	7.25	6.55	13	2.05
30	1.88	0.975	4.47	3.52	3.65	11.3	0.820	17.1	2.05	6.98	3.11	1.28
40	1.80	0.809	2.72	2.29	1.70	4.92	1.70	6.95	1.09	5.80	1.39	0.920
50	1.37	0.965	1.98	1.09	0.885	3.01	1.09	2.65	0.798	2.32	0.715	0.612
60	0.730	0.982	1.68	0.519	0.540	1.69	0.355	1.08	0.825	1.62	0.422	0.411
70	0.340	0.841	1.58	0.328	0.415	0.881	0.271	1.22	1.02	1.92	0.275	0.241
80	0.308	0.743	1.60	0.441	0.338	0.665	0.397	2.50	1.03	2.71	0.200	0.169
90	0.645	0.708	1.79	0.740	0.215	0.620	0.825	2.87	0.900	3.10	0.159	0.141
100	1.21	0.785	2.99	0.870	0.139	0.639	1.25	2.49	0.755	2.91	0.137	0.148
110	1.01	0.910	5.28	0.870	0.150	0.782	1.28	1.59	0.758	2.21	0.136	0.190
120	0.580	0.910	6.44	0.760	0.275	1.31	0.935	1.03	0.845	1.21	0.153	0.260
130	1.31	0.745	7.30	0.840	0.590	2.41	0.320	0.902	1.00	0.911	0.189	0.342
140	3.69	0.641	8.63	1.62	0.942	3.65	0.295	1.28	1.22	0.932	0.255	0.451
(150)	6.60	0.570	10.7	2.91	1.27	4.92	0.720	2.31	1.52	1.30	0.359	0.600
(160)	9.65	0.535	12.9	4.63	1.61	6.41	1.47	4.00	2.22	2.20	0.520	0.770
(170)	12.4	0.500	15.2	6.45	1.99	7.78	2.28	5.61	3.22	3.25	0.720	0.960
(180)	13.6	0.480	17.3	8.00	2.14	8.60	2.85	6.45	4.41	4.12	0.945	1.17
$\sigma_I$	22.5	10.5	57.7	18.7	14.3	46.2	12.7	112	20.4	45.5	50.3	9.49
$\sigma_M$	31.1	9.58	74.2	18.3	8.15	30.3	10.6	29.7	14.4	25.6	4.42	4.59
Error class	C	B	C	B	B	C	C	C	C	C	C	C

TABLE VII. Same as Table II, but for levels 13, 14, and 15.

Angle (deg)	20			30			50			100		
	13 ( $10^{-19}$ )	14 ( $10^{-19}$ )	15 ( $10^{-19}$ )	13 ( $10^{-19}$ )	14 ( $10^{-19}$ )	15 ( $10^{-19}$ )	13 ( $10^{-19}$ )	14 ( $10^{-19}$ )	15 ( $10^{-19}$ )	13 ( $10^{-19}$ )	14 ( $10^{-20}$ )	15 ( $10^{-20}$ )
(0)	1.11	0.345	1.07	0.805	1.24	2.69	17.9	3.50	1.25	62.0	54.5	8.21
10	1.29	0.361	0.771	2.25	1.21	2.45	10.5	2.18	1.23	14.1	13.9	6.30
20	1.97	0.480	0.605	5.61	1.19	2.21	1.15	1.07	1.19	0.845	4.15	4.75
30	4.60	0.718	0.795	9.60	1.18	1.86	3.65	0.890	1.14	2.72	3.00	3.55
40	4.61	1.18	1.43	7.45	1.16	1.48	5.40	0.905	1.06	3.09	2.34	2.62
50	1.76	1.89	2.12	2.81	1.14	1.07	3.85	1.03	0.945	1.55	1.82	1.89
60	0.990	2.73	2.32	0.741	1.19	1.01	1.30	1.11	0.779	0.425	1.40	1.32
70	0.775	2.12	1.80	0.275	1.29	1.50	0.380	1.02	0.618	0.810	1.02	0.865
80	0.905	1.21	1.38	0.700	1.60	2.42	1.55	0.795	0.473	1.22	0.690	0.503
90	1.21	1.46	1.33	1.55	1.89	2.32	3.04	0.480	0.371	1.40	0.450	0.340
100	1.13	1.78	1.67	2.09	1.98	1.23	4.18	0.242	0.302	1.30	0.270	0.278
110	0.275	1.79	1.75	2.02	1.71	0.881	3.97	0.170	0.275	0.881	0.171	0.253
120	0.255	1.98	1.86	1.48	1.79	1.74	2.01	0.415	0.313	0.415	0.122	0.259
130	1.89	3.63	3.58	0.600	2.60	3.55	0.451	0.941	0.461	0.161	0.129	0.292
140	4.10	9.40	6.90	0.960	4.50	5.85	0.365	1.72	0.730	0.395	0.230	0.418
(150)	6.50	16.2	10.9	1.63	7.05	8.10	0.795	2.60	1.06	0.880	0.520	0.875
(160)	8.35	22.8	15.9	2.49	10.0	10.1	1.39	3.50	1.41	1.40	0.975	1.39
(170)	10.1	29.0	19.7	3.41	12.9	11.3	1.93	4.37	1.70	1.89	1.51	1.88
(180)	11.7	35.5	21.0	4.15	14.3	12.2	2.47	4.90	1.85	2.31	2.00	2.31
$\sigma_I$	27.3	49.5	40.0	28.3	30.6	33.5	30.7	12.8	8.42	17.7	15.1	14.2
$\sigma_M$	31.7	75.6	57.6	20.3	41.9	44.6	25.2	14.6	7.74	11.5	6.83	8.05
Error class	A	B	A	A	B	A	A	B	A	A	C	C

TABLE VIII. Same as Table II, but for levels 16, 17, and 18.

Angle (deg)	20			30			50			100		
	16 ( $10^{-19}$ )	17 ( $10^{-19}$ )	18 ( $10^{-19}$ )	16 ( $10^{-19}$ )	17 ( $10^{-19}$ )	18 ( $10^{-19}$ )	16 ( $10^{-20}$ )	17 ( $10^{-20}$ )	18 ( $10^{-20}$ )	16 ( $10^{-20}$ )	17 ( $10^{-20}$ )	18 ( $10^{-20}$ )
(0)	1.07	1.00	1.83	1.73	2.71	6.65	25.0	47.1	201	16.9	42.0	285
10	0.671	0.751	0.929	1.64	2.37	5.03	7.40	35.5	119	8.90	26.5	69
20	0.428	0.461	0.518	1.48	1.89	3.35	3.78	23.5	19.1	2.51	12.9	2.70
30	0.471	0.311	0.428	1.33	1.37	2.05	3.51	14.5	6.27	1.28	4.95	1.28
40	0.720	0.345	0.581	1.15	0.940	1.13	6.18	7.95	5.74	1.02	2.19	1.02
50	1.32	0.535	0.975	1.00	0.615	0.655	6.97	3.28	5.20	0.841	1.13	0.841
60	2.19	0.740	1.51	0.950	0.465	0.490	6.45	1.61	3.28	0.610	0.681	0.585
70	2.03	0.965	1.19	1.02	0.580	0.447	5.85	2.40	1.79	0.382	0.424	0.375
80	1.57	1.00	1.11	1.18	0.720	0.455	4.55	3.08	1.59	0.240	0.275	0.241
90	1.70	1.22	1.52	1.34	0.735	0.473	3.65	3.22	1.88	0.182	0.218	0.181
100	2.31	1.79	2.00	1.43	0.675	0.503	3.05	2.87	2.00	0.160	0.204	0.161
110	2.68	1.82	1.73	1.41	0.640	0.600	2.78	2.02	1.81	0.173	0.221	0.173
120	2.91	1.43	1.59	1.67	0.785	0.785	2.71	1.23	1.24	0.228	0.275	0.226
130	3.81	1.31	2.35	2.28	1.37	1.11	3.05	1.13	0.646	0.325	0.375	0.325
140	5.82	1.63	3.69	3.39	2.25	1.65	4.31	1.65	0.661	0.518	0.529	0.510
(150)	9.10	2.37	5.40	4.58	3.10	2.40	6.78	2.62	1.11	0.825	0.785	0.825
(160)	12.9	3.27	7.25	5.78	3.99	3.20	9.60	3.80	2.03	1.30	1.20	1.29
(170)	17.1	4.25	8.80	6.80	4.61	4.00	12.2	4.95	3.37	1.87	1.71	1.87
(180)	20.1	5.00	9.50	7.10	5.00	4.45	13.9	5.78	4.45	2.41	2.39	2.41
$\sigma_I$	38.7	16.2	24.9	22.9	14.7	14.0	60.4	55.4	61.4	9.03	20.1	24.1
$\sigma_M$	55.4	20.7	34.0	29.4	18.0	14.7	58.5	31.9	22.5	5.99	7.03	6.10
Error class	A	B	A	A	B	B	B	B	B	C	C	C

TABLE IX. Same as Table II, but for levels 19, 20, and 21.

Angle (deg)	20		19		30		19		50		100		21	
	(10 <sup>-19</sup> )	(10 <sup>-20</sup> )	(10 <sup>-19</sup> )	(10 <sup>-19</sup> )	(10 <sup>-19</sup> )	(10 <sup>-20</sup> )								
(0)	1.36	2.02	0.798	12.9	33.0	3.90	91.5	281	200	210	575	3200		
10	1.09	1.78	0.531	9.75	20.0	2.80	37.0	94.0	66.1	35.5	82.0	270		
20	0.740	1.33	0.279	6.15	10.2	1.82	11.8	18.3	12.9	12.9	5.35	2.90		
30	0.470	0.981	0.172	3.60	5.10	1.08	4.15	7.45	6.10	1.63	2.39	0.871		
40	0.398	0.828	0.352	1.80	2.87	0.670	1.72	4.85	4.35	0.691	1.19	0.420		
50	0.455	0.946	0.583	0.815	1.53	0.479	1.03	2.15	3.65	0.259	0.525	0.219		
60	0.680	0.921	0.643	0.435	0.440	0.362	0.481	0.780	3.11	0.110	0.221	0.148		
70	0.805	0.573	0.502	0.315	0.439	0.388	0.222	0.491	2.68	0.069	0.155	0.112		
80	0.638	0.540	0.519	0.205	0.821	0.580	0.238	0.579	2.01	0.090	0.219	0.094		
90	0.529	0.735	0.740	0.119	1.11	1.02	0.398	0.681	1.41	0.118	0.285	0.083		
100	0.640	0.827	1.12	0.120	1.04	1.30	0.515	0.680	0.985	0.130	0.322	0.076		
110	0.443	0.650	1.30	0.221	0.700	0.831	0.515	0.541	0.745	0.121	0.248	0.072		
120	0.395	0.360	1.39	0.371	0.411	0.518	0.418	0.341	0.698	0.099	0.168	0.072		
130	0.645	0.800	2.09	0.585	0.682	1.00	0.210	0.183	0.775	0.082	0.114	0.076		
140	1.03	2.90	3.63	0.803	1.15	2.08	0.185	0.171	0.980	0.084	0.122	0.087		
(150)	1.63	5.53	5.58	1.01	1.65	3.00	0.352	0.315	1.41	0.129	0.250	0.112		
(160)	2.36	8.20	7.60	1.23	2.22	4.02	0.660	0.488	2.08	0.242	0.450	0.169		
(170)	3.13	11.1	9.40	1.39	2.70	5.10	1.07	0.659	2.81	0.400	0.661	0.269		
(180)	3.79	14.2	10.0	1.49	3.00	5.98	1.49	0.845	3.51	0.559	0.820	0.380		
$\sigma_T$	9.41	18.6	19.5	12.3	23.0	14.5	21.1	43.5	44.7	14.7	34.3	110		
$\sigma_M$	11.1	25.9	29.8	6.98	13.7	18.0	6.02	8.16	19.1	1.98	3.74	2.15		
Error class	B	A	B	A	A	B	A	A	C	A	A	C		

TABLE X. Same as Table II, but for levels 22 and 23.

Angle (deg)	20		30		50		100		23	
	(10 <sup>-19</sup> )	(10 <sup>-20</sup> )	(10 <sup>-19</sup> )	(10 <sup>-19</sup> )	(10 <sup>-19</sup> )					
(0)	0.720	2.92	47.1	12.0	79.0	251	758	745		
10	0.725	1.95	24.5	11.2	27.0	101	210	89.0		
20	0.785	1.27	9.15	8.85	6.85	19.8	28.0	6.05		
30	0.915	1.04	3.19	6.00	3.15	8.25	11.3	2.59		
40	1.08	0.971	1.42	3.51	1.73	4.85	5.35	1.45		
50	1.18	0.952	0.825	1.79	1.00	2.28	2.79	0.685		
60	1.20	0.960	0.615	0.855	4.78	0.945	1.67	0.241		
70	1.19	0.825	0.541	0.518	0.452	0.603	1.28	0.112		
80	1.13	0.682	0.518	0.435	0.700	0.805	1.10	0.109		
90	1.07	0.595	0.502	0.411	0.665	0.902	1.02	0.245		
100	1.11	0.561	0.524	0.422	0.513	0.800	1.00	0.445		
110	1.27	0.581	0.598	0.463	0.428	0.563	1.03	0.505		
120	1.52	0.730	0.795	0.618	0.400	0.378	1.06	0.325		
130	1.92	1.17	1.41	0.980	0.435	0.265	1.12	0.141		
140	2.54	1.98	2.85	1.85	0.532	0.271	1.27	0.133		
(150)	3.28	3.00	4.09	3.23	0.681	0.485	1.53	0.219		
(160)	3.98	4.03	5.25	4.92	0.825	1.01	2.09	0.349		
(170)	4.45	5.18	6.30	6.65	1.02	1.93	2.89	0.495		
(180)	4.58	6.01	7.20	7.85	1.20	2.77	3.79	0.600		
$\sigma_T$	19.0	14.6	25.0	23.8	17.8	47.2	87.5	40.0		
$\sigma_M$	23.3	17.6	21.4	18.7	7.74	10.5	19.0	4.33		
Error class	B	A	B	A	B	A	B	A		

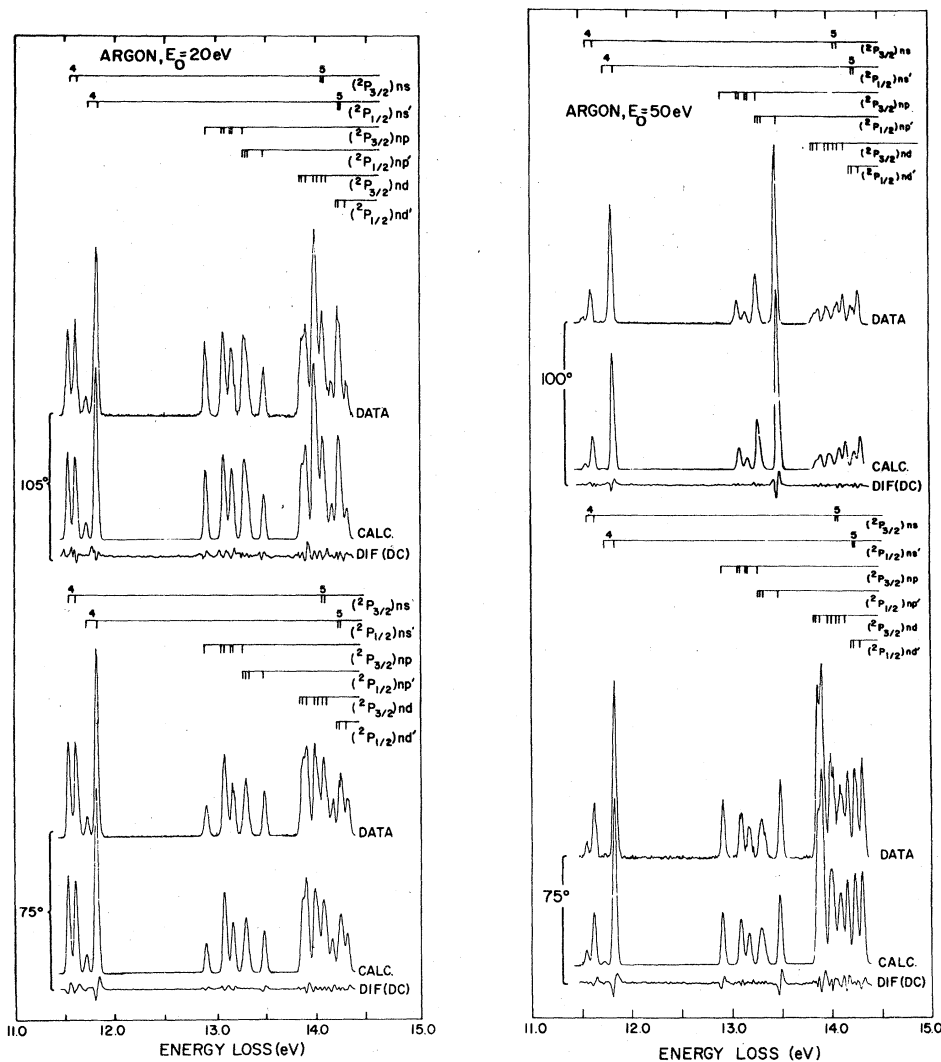


FIG. 1. Representative energy-loss spectra of argon at 20 and 50 eV, at the indicated scattering angles. Rydberg series in the  $ns$ ,  $ns'$ ,  $np$ ,  $np'$ ,  $nd$ , and  $nd'$  orbitals are shown. The line noted as DIF (DC) is the difference spectrum of the raw data and calculated spectrum, and is a measure of the goodness of fit between the calculated and measured argon line intensities.

angular interval. However, in nearly all cases the oscillatory nature of the DCS's is captured. Rather than show plots of all the DCS's given in the tables, only those DCS which could be compared with other experimental data or theories are shown in detail.

#### B. Magnetic sublevel cross sections

Using the measured  $\lambda$  parameters for the 106.7- and 104.8-nm transitions<sup>19,20</sup> and the present results, one may obtain differential magnetic sublevel cross sections for levels 2 and 4. If  $\sigma_0$  is denoted as the sublevel cross section for the  $m=0$ , and  $\sigma_1$  twice that for the  $m=1$  magnetic sublevels

of the two  $J=1$  states, then these quantities are related to the measured DCS ( $d\sigma/d\Omega$ ) by<sup>21</sup>

$$\sigma_0 = \lambda \frac{d\sigma}{d\Omega}, \quad (1)$$

$$\sigma_1 = (1 - \lambda) \frac{d\sigma}{d\Omega}.$$

Measurements of  $\lambda$  have been reported<sup>20</sup> at  $E_0 = 50$  eV and  $\theta = 5^\circ$ . Values of  $d\sigma/d\Omega$  at  $\theta = 5^\circ$  were obtained from the present work by extrapolating (at 50 eV)  $d\sigma/d\Omega$  for levels 2 and 4 from  $10^\circ$  (our lowest-angle measurement) to  $5^\circ$ , using the theoretical FOMBT DCS<sup>25</sup> as a guide. The value for  $d\sigma/d\Omega$  obtained for level 2 was  $3.81 \times 10^{-17}$  cm<sup>2</sup>

## ARGON

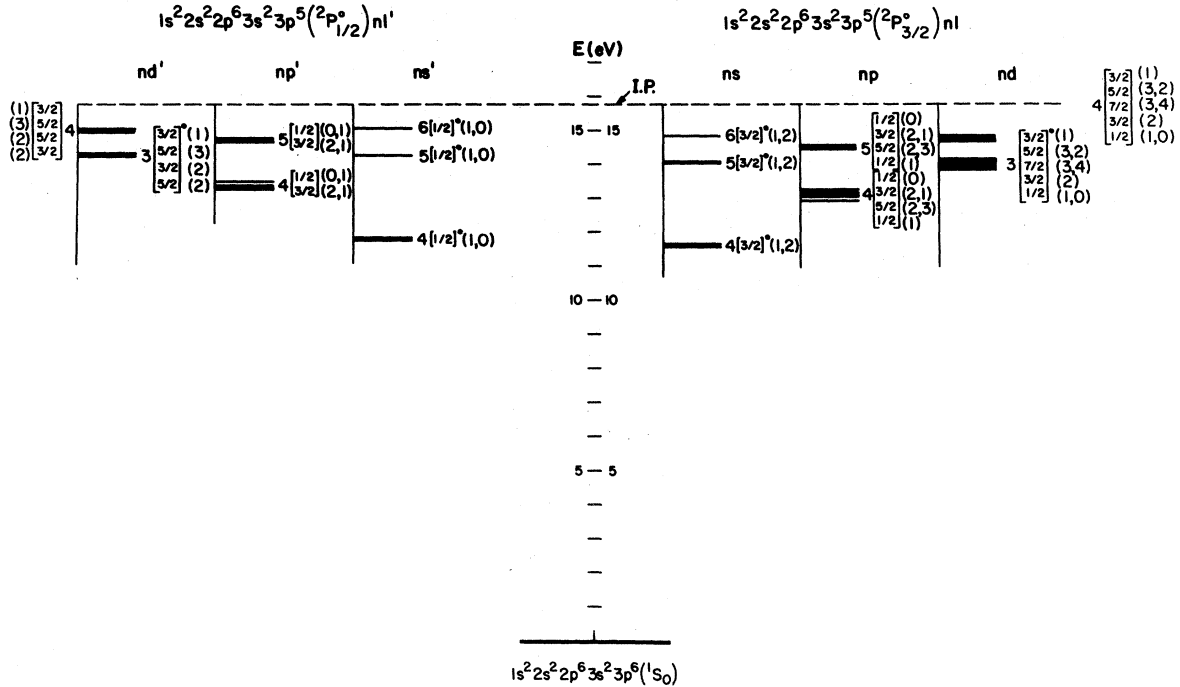


FIG. 2. Grotrian energy-level diagram (Ref. 30) for the levels of argon discussed in the present work. Division is made into the  $s$ ,  $p$ ,  $d$ , and  $s'$ ,  $p'$ ,  $d'$  series corresponding to the  ${}^2P_{3/2}$  and  ${}^2P_{1/2}$  cores, respectively, of Ar II.

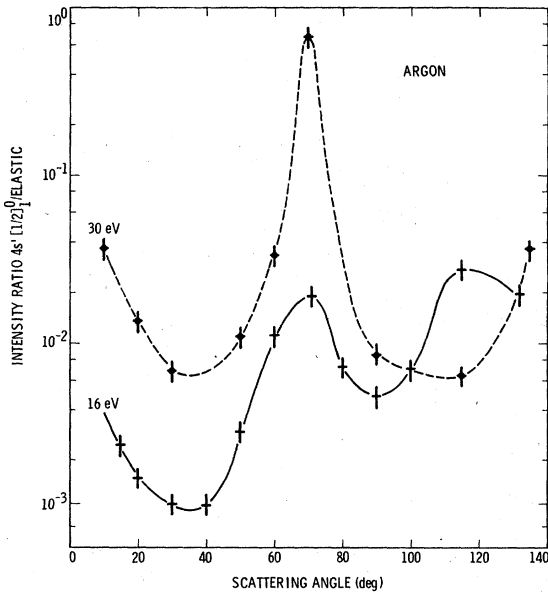


FIG. 3. Intensity ratio of the argon line  $4s' [1/2]_1^0$  (line 4) to the elastic-scattering feature at 16 and 30 eV. Connecting lines are drawn for ease of viewing.

and for level 4 was  $1.42 \times 10^{-16} \text{ cm}^2$ . The corresponding  $\sigma_0$  and  $\sigma_1$  values for level 2 ( ${}^3P_1$ ) are

$$\begin{aligned} \sigma_0 &= (2.29 \pm 0.66) \times 10^{-17} \text{ cm}^2, \\ \sigma_1 &= (1.52 \pm 0.44) \times 10^{-17} \text{ cm}^2, \end{aligned} \quad (2)$$

and for level 4 ( ${}^1P_1$ )

$$\begin{aligned} \sigma_0 &= (1.02 \pm 0.30) \times 10^{-16} \text{ cm}^2, \\ \sigma_1 &= (3.98 \pm 1.15) \times 10^{-17} \text{ cm}^2, \end{aligned} \quad (3)$$

where the errors include the error in  $d\sigma/d\Omega$ , an estimated error in the extrapolation to  $5^\circ$  (10%), and error in the measurement of  $\lambda$  (8.3%).<sup>20</sup> The corresponding theoretical values are<sup>25</sup> [level 2 ( ${}^3P_1$ )]

$$\begin{aligned} \sigma_0 &= 3.18 \times 10^{-17} \text{ cm}^2, \\ \sigma_1 &= 1.36 \times 10^{-17} \text{ cm}^2, \end{aligned} \quad (2')$$

and [level 4 ( ${}^1P_1$ )]

$$\begin{aligned} \sigma_0 &= 1.25 \times 10^{-16} \text{ cm}^2, \\ \sigma_1 &= 5.34 \times 10^{-17} \text{ cm}^2. \end{aligned} \quad (3')$$

The agreement is seen to be satisfactory in the four sublevel cross sections. However, it is interesting to note that the interpretation of the co-

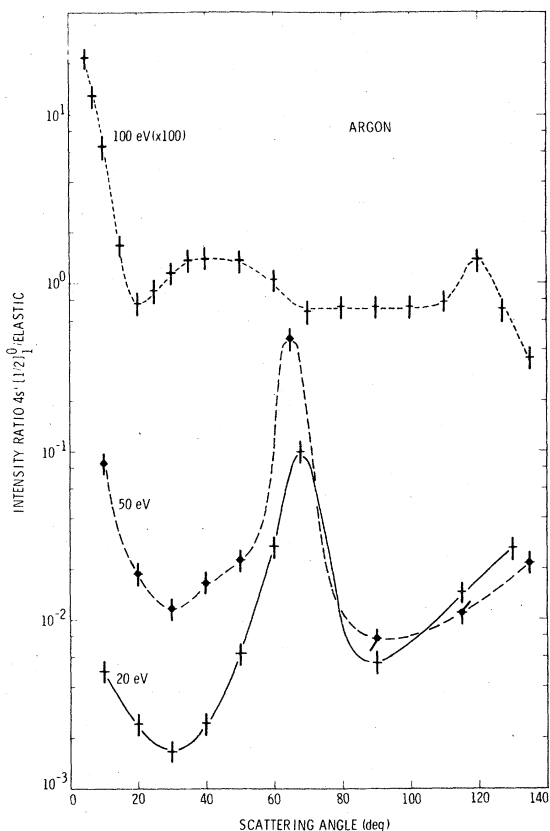


FIG. 4. Same as Fig. 3, but at energies of 20, 50, and 100 eV.

incidence experiment<sup>20</sup> is based on a formula<sup>19</sup> which is valid, in general, only for the  $LS$  coupled case. Recent reinterpretation of the coincidence experiment in the case of spin-orbit coupling<sup>31</sup> has shown a different formula to apply which, for scattering from argon at 50 eV and 5°, gives results fortuitously close to those of the formula used in Ref. 20.<sup>32</sup> A similar decomposition of the  $\lambda$  measurements of Pochat *et al.*,<sup>33</sup> into  $\sigma_0$  and  $\sigma_1$  may be made, with a similar caveat concerning the interpretation of these  $\lambda$ 's.

### C. Integral and momentum-transfer cross sections

Integral cross sections for levels 1 and 3 are shown in Fig. 13, along with results obtained by the FOMBT. Agreement between experiment and theory here reflects to some extent the agreements in the DCS's especially in the 30°–130° angular range which gives the major contribution to the integration (see Figs. 5, 7, 9, and 11).

Integral cross sections for levels 2 and 4 are shown in Fig. 14. In addition to results from the

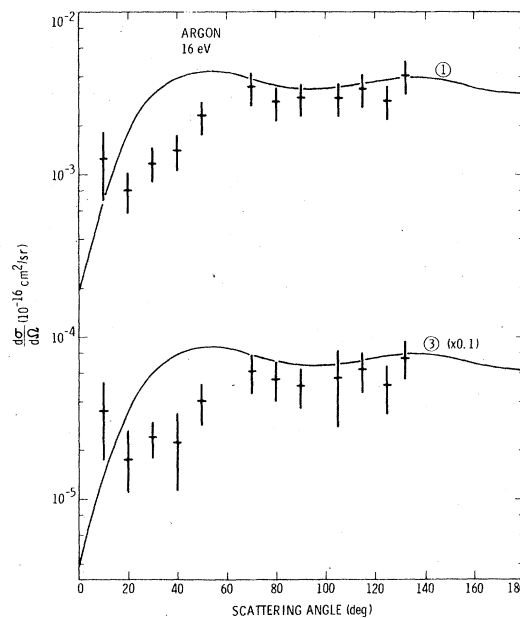


FIG. 5. Experimental (crosses) and theoretical first-order many-body DCS results (solid lines) (Ref. 25) for the first two metastable levels  $1(^3P_2)$  and  $3(^3P_0)$  in argon at 16 eV. The scale change of level 3 refers to both the experimental and theoretical data. This same sense of scale change is used in the subsequent figures.

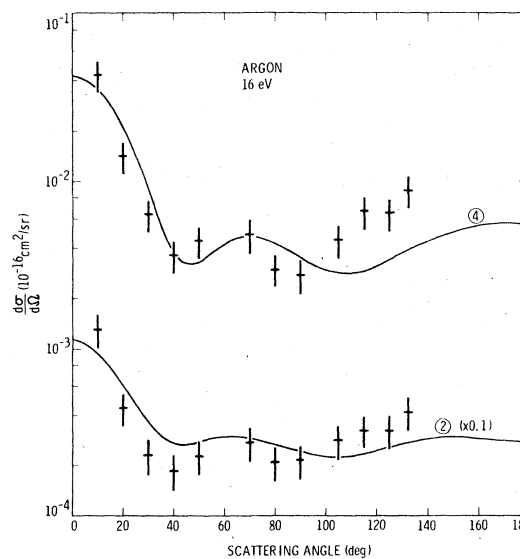


FIG. 6. Experimental (crosses) and theoretical first-order many-body calculation DCS results (solid lines) (Ref. 25) for the first two optically allowed levels  $2(^3P_1)$  and  $4(^1P_1)$  in argon at 16 eV.

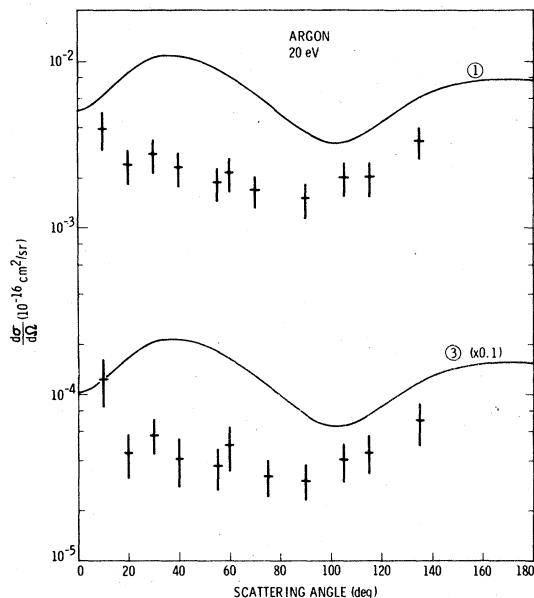


FIG. 7. Same as Fig. 5, but at 20-eV incident-electron energy.

FOMBT the semiempirical Born results of Ref. 22 and, for level 4, optical-excitation data of Ref. 18 corrected for cascade are also shown. The two sets of experimental data for level 4 are in good agreement with one another. Comparison with the semiempirical cross sections shows the latter to be high, by factors of 1.5–2. This trend

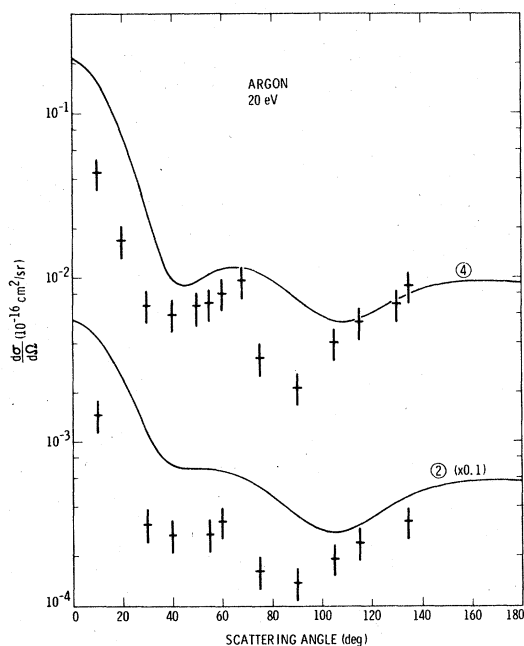


FIG. 8. Same as Fig. 6, but at 20-eV incident-electron energy.

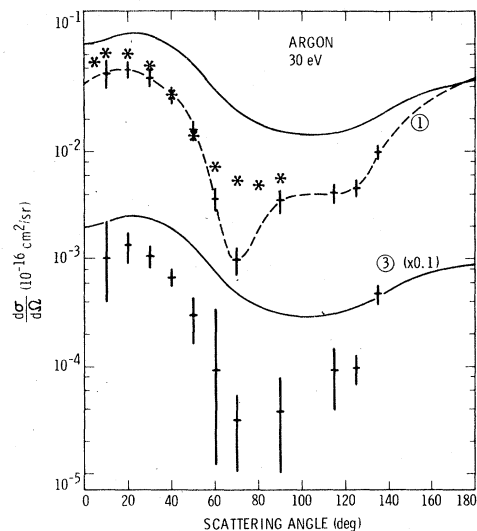


FIG. 9. Same as Fig. 5, but at 30-eV incident energy. The dashed line through the data of level 1 is for ease of viewing. Asterisks (\*) represent relative cross-section results of Ref. 8 which were normalized to the present absolute results at  $\theta = 40^\circ$ .

is also borne out for excitation of the level  $3d'$  [ $3/2$ ]<sub>o</sub> (level 23) to be discussed below. The agreement between results of the FOMBT and experiment is generally better than for the semiempirical results.

Either because of poor experimental resolution, or because spin-orbit coupling effects were not

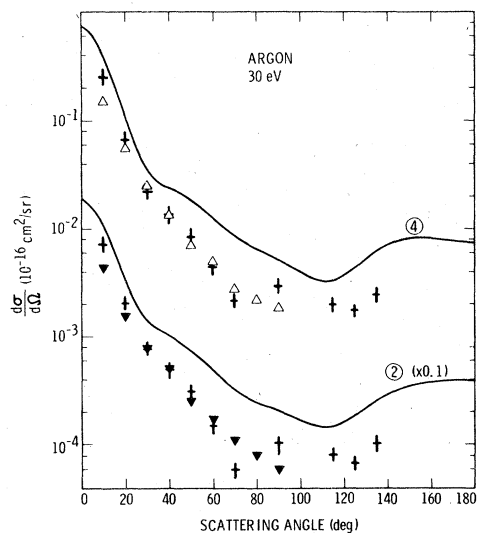


FIG. 10. Same as Fig. 6, but at 30-eV incident electron energy. The open triangles ( $\Delta$ ) are relative DCS of Ref. 8 for level 4 which were normalized to the present absolute results at  $\theta = 40^\circ$ . The filled triangles ( $\blacktriangledown$ ) similarly refer to level 2.

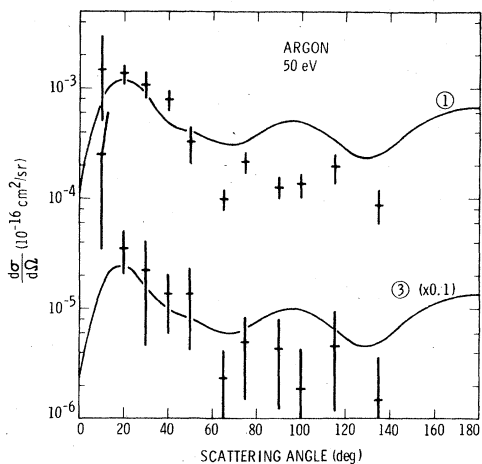


FIG. 11. Same as Fig. 5, but at 50-eV incident electron energy.

included in previous theoretical calculations, levels 2 and 4 are often treated as a single level except for the recent FOMBT calculations. The sum of integral cross sections for excitation of levels 2 and 4 obtained in the present measurements is compared in Fig. 15 with other experiments and theoretical results. There is good agreement between the present data and optical excitation measurements.<sup>18</sup> Results of one other measurement of these combined transitions<sup>34</sup> are plotted

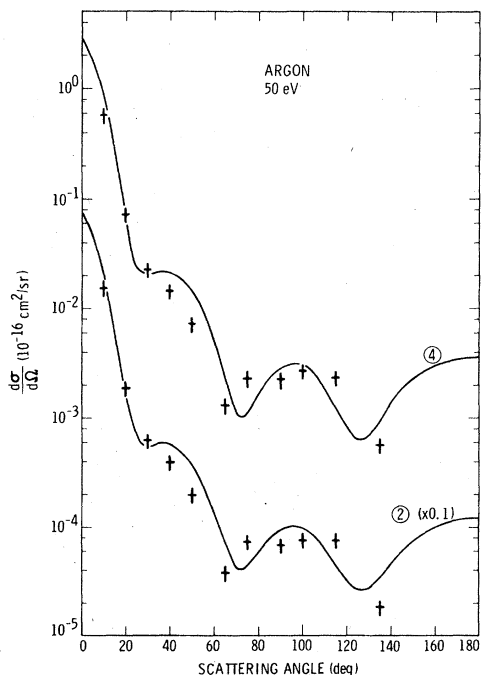


FIG. 12. Same as Fig. 6, but at 50-eV incident-electron energy.

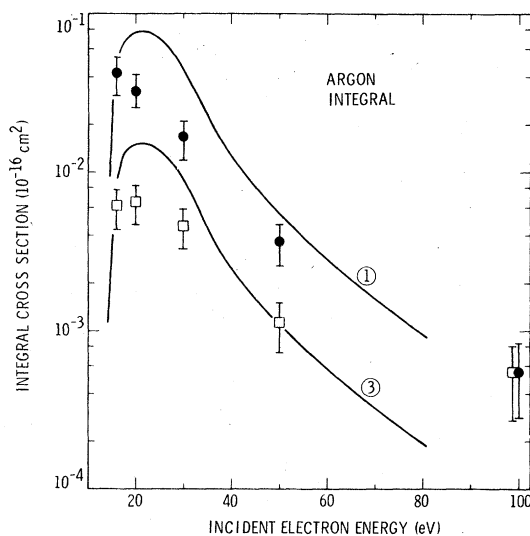


FIG. 13. Integral cross sections for excitation of the metastable levels  $1^3P_2$ , filled circles) and  $3^3P_0$ , open squares). Solid lines are results of the first-order many-body calculation of Ref. 25.

in Fig. 8 of Ref. 18. These results bear the same relationship to our data as to those of Ref. 18 and are not plotted again.

Theoretical results for excitation of these levels include the FOMBT,<sup>25</sup> Born approximation with

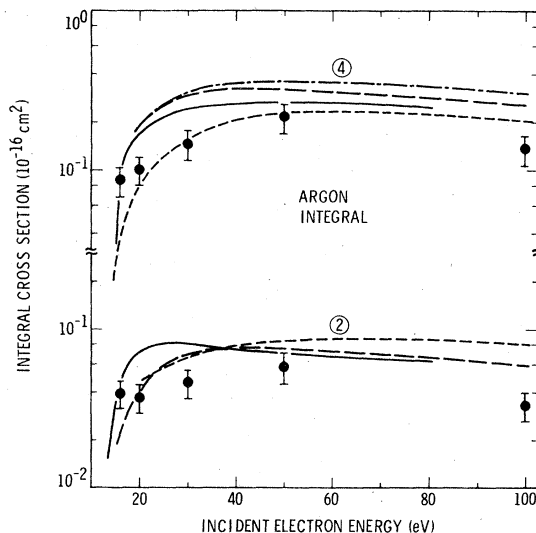


FIG. 14. Integral cross sections for excitation of the optically allowed levels  $2^3P_1$  and  $4^1P_1$ ). Filled circles (●) are present data. Solid lines (—) results of the first-order many-body theory (Ref. 25); long dash lines (—) semiempirical Born calculations (Ref. 22); short dash lines (---) experimental results of Ref. 18 corrected for cascade; dot dash line (·-·-) experimental results of Ref. 17 including cascade. Note break in the ordinate for levels 2 and 4.

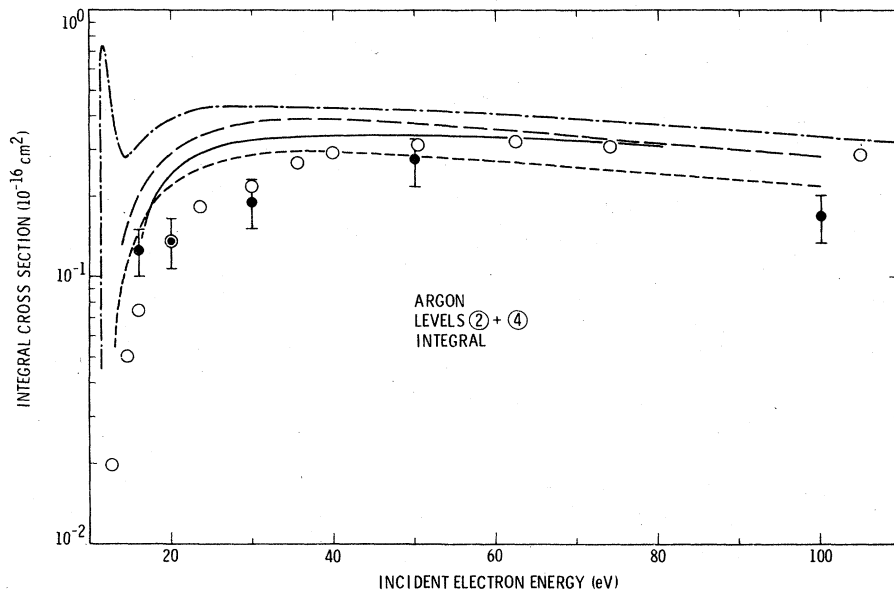


FIG. 15. Sum of integral cross sections for excitation of the optically allowed levels  $2(3P_1)$  and  $4(1P_1)$ . Filled circles (●) are present data and open circles (○) data of Ref. 18. Long dash line (---) results of the Born approximation using one-configuration and frozen core Hartree-Fock wave functions for the ground and excited states, respectively (Ref. 24); short dash line (---) results of the Born approximation using multiconfiguration and fully relaxed wave functions for the ground and excited states, respectively (Ref. 24); dot-dash line (-.-.-) distorted-wave calculation of Ref. 23; solid line (-) results of the first-order many-body theory (Ref. 25).

several ground and excited-state target wave functions,<sup>24</sup> and a distorted-wave (DW) Born calculation.<sup>23</sup> One finds (Fig. 15) good agreement with results from the Born approximation in which a multiconfiguration ground state and fully relaxed excited-state target wave function was used<sup>24</sup>; as well as with results from FOMBT. The sharp peak near threshold for the DW calculation (Fig. 15) is very likely an artifact of the distorting potential used.<sup>23</sup> It is interesting to note that the present measurements show a flattening in the cross section between 16 and 20 eV, perhaps evidence for such a peak. This indication, however, is not statistically significant nor is a peak observed in the optical excitation measurements of Ref. 34.

Several interesting comparisons of the present metastable-level cross sections with other calculations and measurements can also be made. In Fig. 16 the sum of integral cross sections for levels 1 and 3 is shown and compared to results obtained from the FOMBT.<sup>25</sup> The trends here are practically the same as those in Fig. 13 for the individual levels. Again the results from the FOMBT are in reasonably good agreement with experiment. There are also two time-of-flight (TOF) measurements in which the total production of metastable levels was measured as a function of incident electron energy. One is an absolute

measurement from threshold to 50 eV (TOF1)<sup>15</sup> with a stated accuracy of a factor of 2. The other is a relative measurement from 20 to 100 eV (TOF2),<sup>14</sup> the peak of which was normalized here to  $3.55 \times 10^{-17} \text{ cm}^2$ , the average of peak cross sections measured in Ref. 15. First, one sees in Fig. 16 that the results of TOF1 and TOF2 are greater than the present sum of levels 1 and 3, as they should be since they measured the contribution from all metastable levels. Moreover, the cross sections of all resolved metastable levels studied in the present work can be summed to compare to these results. There are 16 levels in all for which  $\Delta J = 0(0 \rightarrow 0)$  and 2, and levels which are of even parity, levels 1, 3, 5-13, 15-18, and 21. This sum (labeled 16 LEVELS) is in good agreement with the TOF results as shown in Fig. 16. However, this curve should still be below the TOF results since (a) unresolved metastable levels (in levels 19 and 22) were not included in the sum, and (b) the present data extended only to an energy loss of 14.3 eV, so that higher metastable levels extending to the ionization limit (15.755 eV) were also excluded from the sum. One concludes then that the detector calibration in the TOF1 measurements should probably place the peak cross sections somewhere in the range  $(3.55 - 7.10) \times 10^{-17} \text{ cm}^2$  to accommodate these missing levels. The curve

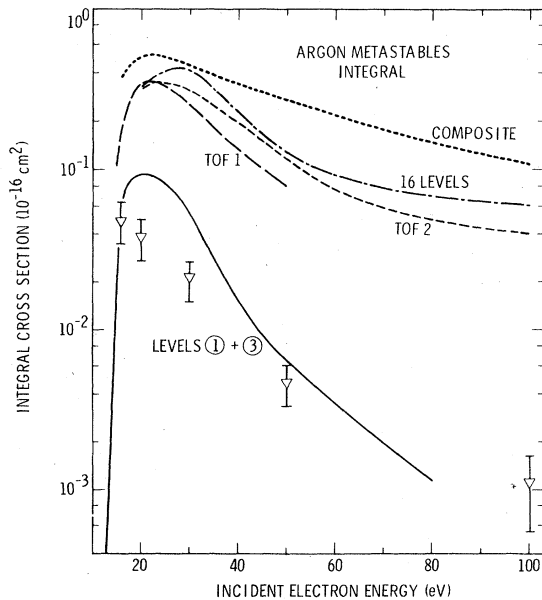


FIG. 16. Integral cross sections for excitation of the metastable argon levels. Experimental data for the sum of cross sections to levels  $1(3P_2)$  and  $3(3P_0)$  are given as open triangles ( $\nabla$ ) for present results; long dash line (---, TOF1) absolute time-of-flight cross sections for excitation of all metastable levels (Ref. 15); short dash line (---, TOF2) relative time-of-flight cross section for excitation of all metastables (Ref. 14) normalized to a peak cross section of  $3.55 \times 10^{-17} \text{ cm}^2$  from Ref. 15; dot-dash line (-.-.-, 16 LEVELS) absolute cross sections for the sum of 16 resolved metastable levels from the present work; dotted line (....., COMPOSITE) composite forbidden cross sections from the semiempirical form of Ref. 22. Solid line is the theoretical first-order many-body calculation (Ref. 25) for the sum of levels 1 and 3.

labeled COMPOSITE is the sum of all metastable cross sections from the semiempirical formula of Ref. 22. It appears to overestimate the metastable cross sections for energies greater than about 40 eV.

One further application of the present integral cross sections is illustrated by results for levels 12 and 23 shown in Fig. 17. The argon transition  $3d'[3/2]_1^0 \rightarrow 4p'(1/2)_1$  is one of two lasing transitions excited in direct nuclear-pumped laser systems.<sup>2,3</sup> In the absence of actual data, modelers have been accustomed to using Born semiempirical cross sections<sup>22</sup> (solid line in Fig. 17) for calculating the electron excitation rate of the upper level 23. One sees a discrepancy of about a factor of 4 between the present data and the semiempirical results. The latter tend to overestimate the

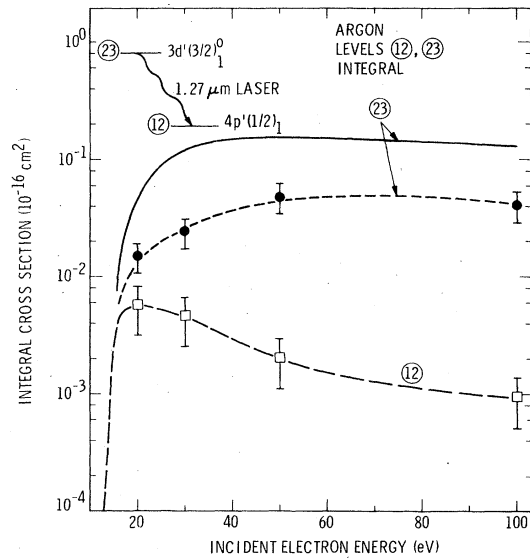


FIG. 17. Present integral cross sections for excitation of the levels  $4p'(1/2)_1$  (level 12, open squares) and  $3d'[3/2]_1^0$  (level 23, filled circles). Dashed connecting lines are for ease of viewing. Solid line represents semiempirical Born calculation of Ref. 22 for level 23. The transition  $23 \rightarrow 12$  is one frequently excited in nuclear-pumped laser systems containing argon (Refs. 2 and 3).

excitation rate, as was noted in Fig. 14 for levels 2 and 4. One other interesting point in Fig. 17 is that the excitation rate to the upper level 23 is 3 to 45 times that to the lower level 12, depending on the electron energy. Hence, all things being equal, one would expect greater lasing efficiency for the  $1.27\text{-}\mu\text{m}$  lasing transition at higher ambient electron energies ( $\sim 100 \text{ eV}$ ) rather than at lower ( $\sim 20 \text{ eV}$ ).

Listings of all the integral and momentum-transfer cross sections are given in Tables II-X. While the DCS are given in only  $10^\circ$  intervals, the interval used for the numerical integrations was  $5^\circ, 2.5^\circ$  or  $1^\circ$  depending upon the slope of the DCS.

#### ACKNOWLEDGMENTS

We would like to thank Dr. D. Ton-That for his integral cross sections in the Born approximation prior to publication. This paper represents one phase of work supported by the National Aeronautics and Space Administration under Contract NAS7-100 to the Jet Propulsion Laboratory, California Institute of Technology; and by the U.S. Department of Energy, under Contract W-7405-eng-36 to Los Alamos Scientific Laboratory, University of California.

- <sup>1</sup>Ch. Brau, in *Excimer Lasers*, Topics in Applied Physics, edited by Ch. K. Rhodes (Springer, Berlin, 1979), Vol. 30, p. 87.
- <sup>2</sup>R. J. DeYoung, N. W. Jalufka, and F. Hohl, *AIAA J.* **16**, 991 (1978).
- <sup>3</sup>N. W. Jalufka, R. J. DeYoung, F. Hohl, and M. D. Williams, *Appl. Phys. Lett.* **29**, 188 (1976).
- <sup>4</sup>H. A. Hyman, *Phys. Rev. A* **18**, 441 (1978); J. H. Jacob and J. A. Mangano, *Appl. Phys. Lett.* **28**, 724 (1976); I. A. Ismael and A. A. Garamoon, *J. Phys. D* **12**, 1117 (1979).
- <sup>5</sup>L. G. Christophorou, D. R. James, and R. A. Mathis, *J. Phys. D* **12**, 1223 (1979).
- <sup>6</sup>Preliminary accounts of this work were presented at the Fifth International Conference on Atomic Physics, Berkeley, 1976, *Abstracts of Fifth International Conference on Atomic Physics*, edited by R. Mavrus, M. H. Prior, and H. A. Shugart (Berkeley, 1976), p. 383, and at the Tenth International Conference on Phys. Elect. Atomic Collisions Paris, 1977, *Abstracts of Tenth ICPEAC*, edited by M. Barat and J. Reinhardt (Commissariat à l'Énergie Atomique, Paris, 1977), p. 432.
- <sup>7</sup>C. E. Moore, *Atomic Energy Levels*, (National Bureau of Standards Circular 467, Washington, 1949), Vol. I, p. 211.
- <sup>8</sup>W.-C. Tam and C. E. Brion, *J. Electron Spectrosc. Relat. Phenom.* **2**, 111 (1973).
- <sup>9</sup>B. R. Lewis, E. Weigold, and P. J. O. Teubner, *J. Phys. B* **8**, 212 (1975).
- <sup>10</sup>T. Tsuboi, N. Oda, and Y. Hatano, *Chem. Phys. Lett.* **37**, 499 (1976).
- <sup>11</sup>E. N. Lassettre, A. Skerbele, M. A. Dillon, and K. J. Ross, *J. Chem. Phys.* **48**, 5066 (1968).
- <sup>12</sup>J. Olmsted III, A. S. Newton, and K. Street, Jr., *J. Chem. Phys.* **42**, 2321 (1965).
- <sup>13</sup>S. E. Kuprianov, *Opt. Spektrosk.* **20**, 163 (1966) [*Opt. Spectrosc. (USSR)* **20**, 85 (1966)].
- <sup>14</sup>C. R. Lloyd, E. Weigold, P. J. O. Teubner, and S. T. Hood, *J. Phys. B* **5**, 1712 (1972).
- <sup>15</sup>W. L. Borst, *Phys. Rev. A* **9**, 1195 (1974).
- <sup>16</sup>I. P. Zapesochnyi and P. V. Feltsan, *Opt. Spektrosk.* **20**, 521 (1966) [*Opt. Spectrosc. (USSR)* **20**, 291 (1966)]; J. K. Ballou, C. C. Lin, and F. E. Fajen, *Phys. Rev. A* **8**, 1797 (1973).
- <sup>17</sup>J. E. Mentall and H. D. Morgan, *Phys. Rev. A* **14**, 954 (1976).
- <sup>18</sup>J. W. McConkey and F. G. Donaldson, *Can. J. Phys.* **51**, 914 (1973).
- <sup>19</sup>M. Eminyan, K. B. MacAdam, J. Slevin, and H. Kleinpoppen, *J. Phys. B* **7**, 1519 (1974).
- <sup>20</sup>I. C. Malcolm and J. W. McConkey, *J. Phys. B* **12**, 511 (1979).
- <sup>21</sup>A. Chutjian and S. K. Srivastava, *J. Phys. B* **8**, 2360 (1975); A. Chutjian, *ibid.* **9**, 1749 (1976).
- <sup>22</sup>L. R. Peterson and J. E. Allen, Jr., *J. Chem. Phys.* **56**, 6068 (1972). Another semiempirical approach is used by E. Eggarter [*J. Chem. Phys.* **62**, 833 (1975)] but comparisons here will be restricted to the work of Peterson and Allen.
- <sup>23</sup>T. Sawada, J. E. Purcell, and A. E. S. Green, *Phys. Rev. A* **4**, 193 (1971).
- <sup>24</sup>D. Ton-That and L. Armstrong, Jr., *Bull. Am. Phys. Soc.* **24**, 775 (1979) and private communication.
- <sup>25</sup>N. T. Padial, G. D. Meneses, F. J. da Paixão, Gy. Csanak, and D. C. Cartwright, *Phys. Rev. A* **23**, 2194 (1981), following paper.
- <sup>26</sup>Gy. Csanak, H. S. Taylor, and R. Yaris, *Adv. At. Mol. Phys.* **7**, 287 (1971).
- <sup>27</sup>D. C. Cartwright, A. Chutjian, S. Trajmar, and W. Williams, *Phys. Rev. A* **16**, 1013 (1977).
- <sup>28</sup>A. Chutjian, *J. Chem. Phys.* **61**, 4279 (1974); *Rev. Sci. Instrum.* **50**, 347 (1979).
- <sup>29</sup>S. K. Srivastava, H. Tanaka, A. Chutjian, and S. Trajmar, *Phys. Rev. A* **23**, 2156 (1981), first paper in this series.
- <sup>30</sup>S. Bashkin and J. O. Stoner, *Atomic Energy-Level and Grottrian Diagrams*, (North-Holland, Amsterdam, 1978), Vol. II.
- <sup>31</sup>K. Blum, F. J. da Paixão, and Gy. Csanak, *J. Phys. B* **13**, L257 (1980).
- <sup>32</sup>F. J. da Paixão, N. T. Padial, Gy. Csanak, and K. Blum, *Phys. Rev. Lett.* **45**, 1164 (1980).
- <sup>33</sup>A. Pochat, F. Gelebart, and J. Peresse, *J. Phys. B* **13**, L79 (1980).
- <sup>34</sup>P. J. O. Teubner, C. R. Lloyd, E. Weigold, and S. T. Hood, *J. Phys. B* **5**, L44 (1972).